Simulation of Polyethylene Thin Films on a High Coordination Lattice

Pemra Doruker and Wayne L. Mattice*

Institute of Polymer Science, The University of Akron, Akron, Ohio 44325-3909

Received September 8, 1997; Revised Manuscript Received December 1, 1997

ABSTRACT: We present the results of some film simulations of polyethylene (PE) on a coarse-grained lattice, which is termed as the second nearest neighbor diamond (2nnd) lattice. Monte Carlo simulations of PE melts have been performed on the 2nnd lattice by including short- and long-range interactions. Films can be obtained from equilibrated bulk snapshots by increasing one periodic side to infinity. The presence of attractive long-range interactions besides the repulsive ones gives a cohesive nature to the film. PE films, which contain up to 108 chains of C_{99} and have thicknesses of more than 100 Å between the two surfaces, can be produced and equilibrated on the 2nnd lattice. In these films, the density profiles are hyperbolic, with end beads being more abundant than the middle beads at the interface. There are orientational preferences at the interface on the scale of individual bonds and whole chains. The center of mass distribution of the chains exhibits oscillatory behavior. A comparison of films with different thicknesses, which contain different number of chains, does not indicate any significant differences in local and global equilibrium properties. At lower temperatures, the interfaces get sharper and the orientational preferences are more pronounced. Surface energies close to experimental values are calculated directly from the on-lattice energetics. It is also possible to reverse map equilibrated snapshots from the lattice back to the atomistic model and minimize their energy. The energetics of the resulting film snapshots in continuous space seem to be in agreement with the experimental data on PE.

Introduction

Computer simulations are a useful tool for understanding the equilibrium and dynamic properties of surfaces at the molecular level. In this study, we will specifically deal with the modeling of the surfaces a polyethylene (PE) melt presents to a vacuum.

First lattice simulations of a melt-vacuum interface were performed by Madden[1] using a film adsorbed on a solid surface. Off-lattice Monte Carlo (MC) simulations were later performed on films of a bead−spring homopolymer system by Kumar *et al.*[2] In this MC study, a hypothetical plane, called "the Gibbs dividing plane" was shown to separate the liquid- and gas-side regions around the interface. It was shown[2] that the chains on the liquid-side exhibit meltlike characteristics near a hard wall, whereas the chains assume more collapsed configurations on the gas-side. Molecular dynamics (MD) simulations were also performed on films of short-chain alkanes, namely C_{10} and C_{20}.[3] The results of these fully atomistic simulations qualitatively agree with the MC simulations of model systems of flexible chains.

A glassy atactic polypropylene (PP) surface was simulated fully atomistically by using a molecular mechanics technique,[4] in which a set of static microstates is generated. Then, the short time scale dynamics of this atactic polypropylene−vacuum interface was studied using MD simulations.[5]

MD simulations of thin films formed by single chains of one hundred monomers were performed with different polymers, such as poly-(1,4-cis-butadiene) (*cis*-PDB)[6] and amorphous PE.[7] However, the thickness of the films produced by MD simulations is quite small, less than 40 Å between the two free surfaces. Therefore, the films consist mainly of two interface regions with the density in the center of the film approaching the bulk polymer density at the specific temperature. It is still possible to analyze the local interfacial properties, such as the orientation of bonds and the distribution of torsional angles. Surface energy estimates close to experimental ones were also obtained[6,7] by comparison with bulk simulations. However, it is impossible to fully atomistically simulate larger films with a thicker cross section and/or for a longer time, to analyze the global equilibrium properties and/or the dynamics of chains. In this respect, coarse-grained simulations of specific polymer melts might be an alternative approach in filling the gap between the MC simulations of flexible model systems and the fully atomistic simulations of comparatively smaller systems.

In recent work, a dynamic Monte Carlo (MC) simulation method on a new high coordination lattice has been introduced.[8] This lattice is formed by connecting every other lattice site on a diamond lattice. It is called the "second nearest neighbor diamond" (2nnd) lattice. First simulations on this coarse-grained lattice have been performed with single chains of PE[9] and poly(ethylene oxide)[10] using the rotational isomeric state (RIS) model.[11,12] After the incorporation of long-range interactions, bulk PE simulations have been successful on the 2nnd lattice.[13,14] The simulations are efficient due to the following facts: (i) each lattice site accommodates two backbone atoms, (ii) the occupancy of the lattice is low (<20%), (iii) each accepted move changes the coordinates of one bead on the 2nnd lattice (but there are 2−3 carbon atoms and the values of 3−5 torsions in the underlying atomistic model),[14] and (iv) the continuous Lennard−Jones potential is replaced by a step function.[13] It is also possible to reverse map specific snapshots back to the atomistic model, i.e., continuous space, during the course of the simulations. Therefore, this method also serves as a useful basis for the equilibration of large bulk systems, which is impossible to carry out by fully atomistic simulations.

In this work, we will describe how this specific MC simulation technique could be used to produce equilibrated PE thin films, which have larger system sizes than those obtained by fully atomistic simulations. It is possible to form thin films on the 2nnd lattice, because

S0024-9297(97)01322-3 CCC: $15.00 © 1998 American Chemical Society
Published on Web 01/31/1998

attractive long-range interactions are present besides the repulsive interactions among nonbonded sites on the lattice. PE films of ~2500 Å^2 periodic area and >100 Å thickness between two surfaces are formed and equilibrated easily. Films that contain up to 108 chains with 50 coarse-grained bonds on the 2nnd lattice ($C_{99}H_{200}$ when reverse mapped) have been formed.

In the next section, a brief introduction to the simulation method will be given. Then the simulation parameters and the different techniques of film formation will be described. The results and discussion part comprises of three sections: (i) analysis of two PE films of different thickness (36 and 72 chains of C_{99}); (ii) Analysis of two films at different temperatures (36-chains of C_{99} at 400 and 509 K); (iii) Analysis of some reverse-mapped and energy-minimized snapshots from a film containing nine chains of C_{99}. In all discussions, we will mainly focus on the local and global equilibrium characteristics of the films. The last section will present the concluding remarks.

Model and Method

The 2nnd lattice has a coordination number of 12. The 2nnd unit cell is a slanted cell with an angle of 60° between any two of the x', y', and z' axes passing through the sides of the slanted cell. The lattice sites are identical to the hexagonal packing of hard spheres. However, the term "2nnd lattice" is specifically chosen due to the underlying diamond lattice, which is a natural choice for the mapping of PE. Each 2nnd lattice site accommodates two backbone carbons plus the side-chain hydrogens in the case of PE. Dynamic Monte Carlo simulations are performed after mapping the chains on this coarse-grained lattice. In the simulations, each Monte Carlo Step (MCS) corresponds to a series of single bead moves, where all the beads in the system are randomly attempted for movement. The details of the different moves, which correspond to the displacement of two or three backbone atoms on the real PE chain, can be found in ref 14.

Energetics. The short-range interactions that determine the local conformational preferences of polymers are introduced by using the rotational isomeric state (RIS) formalism.[11,12] The classical RIS model for PE has been modified for the 2nnd lattice[9] by determining the probabilities and conditional probabilities for the coarse-grained states on the lattice. The original first- and second-order interaction energy parameters of Abe *et al.*[15] are used in driving the coarse-grained probabilities for PE. Reference 9 describes the adaptation of these short-range interactions to use on the 2nnd lattice.

The long-range intramolecular and intermolecular interaction energies between nonbonded lattice sites are originally derived from the spherically symmetric Lennard Jones (LJ) potential for ethylene units (CH_2═CH_2), which is used in place of the unknown potential for CH_2−CH_2. In this derivation, the second virial coefficient expression is used to determine an average interaction energy for each shell of neighbors around a lattice site. The intramolecular long-range interactions act between lattice sites separated by more than two 2nnd bonds. Self-avoidance and mutual avoidance as applied to all beads. Details for determining the long-range energies can be found in ref 13. Table 1 summarizes three different sets of long-range parameters employed in the film simulations. Set I is derived from the LJ parameters of ethylene units with respective energy and length parameters of ϵ/k = 205 K and σ = 4.2 Å.[16] (k stands for the Boltzmann constant.) Sets II and III are obtained by changing ϵ and/or σ values for ethylene units within acceptable ranges. The upper limit for the variations could be the parameters for ethane, which are ϵ/k = 230 K and σ = 4.4 Å.[16] (Each set of interaction energies (u_1,u_2, ... u_5) are obtained by the performing the averaging procedure at 443 K.)

Table 1. Long Range Interaction Energy Parameter Sets Used in PE Simulations

	set I	set II	set III
ϵ/k (K)	205	185	205
σ (Å)	4.2	4.4	4.4
u_1 (kJ/mol)[a]	12.501	14.122	14.215
u_2	0.084	0.526	0.429
u_3	−0.611	−0.627	−0.699
u_4	−0.137	−0.155	−0.172
u_5	−0.036	−0.041	−0.045

[a] The long-range interaction energies for the first five shells on the 2nnd lattice (u_1, u_2, ... u_5) are derived using the different sets of LJ parameters (ϵ and σ) at 443 K.

The resulting average interaction energy between two first neighbors on the 2nnd lattice (u_1) is highly repulsive in all parameter sets. This is due to the fact that one 2nnd lattice spacing (between two first neighbors) is 2.5 Å for PE (the bond length of a C−C bond is 1.53 Å, and the angle between two adjacent C−C bonds is tetrahedral on the underlying diamond lattice), which is significantly smaller than σ for ethylene units and falls into the repulsive part of the LJ interactions. The second shell interaction energy (u_2) between beads separated by two 2nnd bonds (42 second neighbors exist around a specific site) averages the repulsive and attractive parts of LJ potential and is slightly above zero. The third shell energy (u_3) is the major attractive one, whereas the fourth and fifth shell energies (u_4 and u_5), being still negative but getting close to zero, correspond to the attractive tail of the LJ potential. In the simulations, we calculate the long range energies from the first three shells, neglecting the fourth and fifth shells. Incorporation of the attractive third shell energy, which brings about the cohesion for the system, makes it possible to perform thin film simulations on the 2nnd lattice. If only the first two shell energies were used, it would be impossible to form films on this lattice.

Film Formation. Two different procedures are employed for the formation of films. The first procedure is an adaptation of the method of Misra *et al.*[6] to lattice simulations. In this procedure, first bulk simulations are performed, which are periodic in the x', y', and z' directions of the 2nnd lattice. After the bulk system has equilibrated, the number of lattice sites on one of the directions, which will be referred as z' in this work, is increased 3−4 times the original number. If the bulk system is equilibrated with the parent box located at z_0' to z_p' along the z' axis, the new parent box is from z_0' to z_n', with $z_n' > z_p'$. The image of each parent chain that is retained for the subsequent film simulation is the one with the most beads between z_0' and z_p'. Increasing the lattice sites by 3−4 times practically means that the chains can no longer interact in the z' direction; i.e., the system is periodic in two dimensions (x' and y') only from this point on. After proper equilibration of the newly formed film, equilibrium properties of the films are analyzed. This specific method of film formation will be referred to as the "elongation method" in the following discussions.

The second method by which new films are formed is "the healing method" of two films. A specific snapshot from an equilibrated film is duplicated by shifting the coordinates in the z' direction, such that no two beads from the separate films collapse at the same lattice site, but at least one pair of beads from different films exists as first neighbors of each other. This means that the duplicates are barely touching each other, so that the attractive interactions between the closer regions from the two films will drive the films to merge and form a single film by the diffusion of the chains. The finally equilibrated film will have the same bulk density as the originally duplicated film and will be thicker in the z' direction, containing twice the number of chains as the original film. It is possible to merge two films containing different number of chains (or different snapshots of the same film) if both have the same number of periodic lattice sites in x' and y' directions, i.e., a periodic cross-sectional area.

Table 2. Details of Thin Film Simulations

run	no. of chains	no. of cells[a]	temp (K)	param set	equilibn[b] (×10⁶ MCS)	analysis (×10⁶ MCS)
1	108	21 × 22	509	II	0.5 (H)	0.5
2	72	21 × 22	509	II	1.5 (H)	1.5
3	36	21 × 22	509	II	1.5 (E)	1.5
4	36	21 × 22	443	II	1.0 (R)	0.5
5	36	21 × 22	400	II	1.5 (R)	1.5
6	36	21 × 22	509	III	0.5 (R)	0.5
7	36	21 × 22	400	III	0.5 (R)	0.5
8	9	13 × 13	443	I	2 (E)	6

[a] Number of cells along the x' and y' axes of the 2nnd cell. [b] Equilibration period of the runs. The letter in paranthesis indicates the method of film formation. Key: E, elongation; H, healing; R, reequilibration of a film snapshot at a different temperature or with a different parameter set. Equilibration periods of 1.5×10^6 MCS are performed for runs 2, 3, and 5 in Table 2, which are mainly analyzed in the Results and Discussion section.

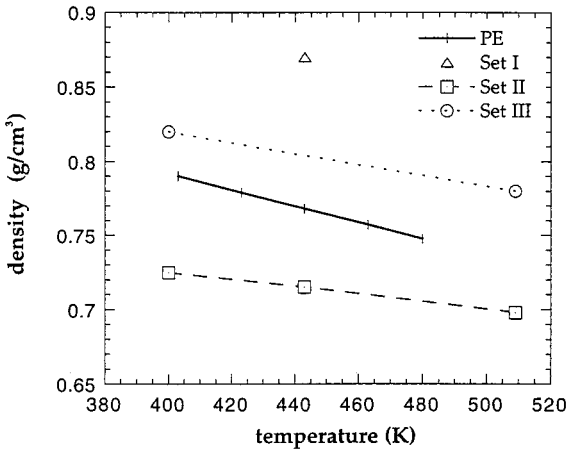

Figure 1. Bulk density of polyethylene (PE) films on the 2nnd lattice as a function of temperature, using three different long-range parameter sets. The lines are drawn to show the temperature dependence more clearly. The darker solid line displays the experimental density of amorphous PE from ref 17.

After a specific film is equilibrated, it is possible to alter the simulation conditions, such as the temperature or the set of energy parameters, and reequilibrate the film at this new set of conditions and analyze the results.

Table 2 summarizes thin film simulations performed on the 2nnd lattice. The simulations are carried out using different long-range parameter sets, which determine the bulk density of the film at the specific temperature. In all the simulations, the chains are made of 50 beads on the 2nnd lattice, which correspond to $C_{99}H_{200}$ after reverse mapping back to the diamond lattice. The number of lattice cells in the periodic x' and y' directions of the simulation box is 21 by 22 in all of the simulations with the exception of run 8. These numbers correspond to periodic dimensions of 52.5 Å × 55 Å with a 60° angle between the x' and y' axis. Run 8 is a relatively smaller system, which is used in the reverse mapping of various snapshots and subsequent energy minimization.

Results and Discussion

The bulk density that the films adopt at a certain temperature does not depend on the number of chains in the system, if the film contains enough chains to exhibit a bulk region. For example, simulations carried out with 36, 72, and 108 chains (the first three entries in Table 2) all have a bulk density of ~0.7 g/cm³ with parameter set II. Therefore, in Figure 1 the bulk densities of thin films at different temperatures are plotted irrespective of the system size. The dark solid line represents the data obtained from an estimate of the amorphous density of polyethylene in the temperature range of 130−207 °C.[17] It is evident that different sets of long-range parameters lead to different bulk densities on the 2nnd lattice. Specifically, the parameter set I derived from the LJ potential of ethylene leads to a quite high bulk density at 443 K. Among the parameter sets considered in Table 2, set II ($\epsilon/k = 185$ K and $\sigma = 4.4$ Å) seems to be the best choice for PE. In Table 3, the overall chain dimensions and the interfacial thickness of the films are reported.

Table 3. Thin Film Simulation Results

run	temp[a] (K)	$\langle r^2 \rangle$[b] (Å²)	$\langle R_g^2 \rangle$[c] (Å²)	interfacial thickness[d] (Å)
1	509 (108, II)	1102	179	11.9
2	509 (72, II)	1144	182	12.1
3	509 (36, II)	1106	178	12.2
4	443 (36, II)	1146	185	10.7
5	400 (36, II)	1295	200	9.6
6	509 (36, III)	1110	174	10.3
7	400 (36, III)	1070	181	8.5
8	443 (9, I)	1057	172	7.5

[a] This column gives a summary of simulation parameters from Table 2. The first and second numbers in parentheses represent the number of chains and the long-range parameter set, respectively. [b] $\langle r^2 \rangle$ stands for the mean squared end-to-end distance of the chains. Standard deviations among the $\langle r^2 \rangle$ values for each chain in the system are calculated as 208, 197, and 463 Å² for runs 2, 3, and 5, respectively. [c] $\langle R_g^2 \rangle$ stands for the mean squared radius of gyration of the chains. Standard deviations among the $\langle R_g^2 \rangle$ values for each chain in the system are calculated as 22, 23, and 51 Å² for runs 2, 3, and 5, respectively. For the eight entries in this table, the average value of $\langle r^2 \rangle / \langle R_g^2 \rangle$ is 6.22 ± 0.17. [d] Interfacial thickness gives the distance over which the density of the film decreases from 90% to 10% of its bulk value, as reported in ref 3. These values are calculated after fitting a hyperbolic tangent function to the interface, which has the same form as in ref 2.

1. Two Films with Different Thicknesses. In this section, we will compare the equilibrium properties of the second and third runs of Table 2. Films in runs 2 and 3 will be distinguished by the number of chains as f72 and f36, respectively, in the following discussions. Both films have the same periodic cross-sectional area of 2501 Å² (21 × 22 cells). Initially, bulk simulations of 36 chains is performed in a box of 21 × 22 × 22 lattice cells at 509 K ($\rho = 0.745$ g/cm³). After 3.5×10^6 MCS steps of bulk simulation, which ensures equilibration (the center of mass movement of the chains is about one radius of gyration in 200 000 MCS on the average), the z'-dimension of the box is increased 3-fold according to the elongation method of film formation. Then, the f36 film is equilibrated using the new periodic boundaries. The f72 film is formed using the healing method after duplicating a snapshot from the f36 film in the z' direction. The interfaces of the films generated on the 2nnd lattice are not normal to the z' axis of the lattice, since the z' axis is slanted. If we denote the XY plane of the Cartesian coordinate system to be coplanar to the 2nnd $x'y'$ plane, the interfaces will be normal to the Z axis of the Cartesian system. Therefore, the Z axis will be used as the basis in the analysis of film profiles. And $Z = 0$ will coincide with the film center of mass in the Z direction.

Density Profiles. Figure 2a shows the density profile of each film from its center of mass. It is calculated by counting the number of backbone carbon atoms (after reverse mapping) that fall into bins of 2 Å thickness on both sides of the film center of mass ($Z = 0$). The bulk density of both films is ~0.7 g/cm³. The

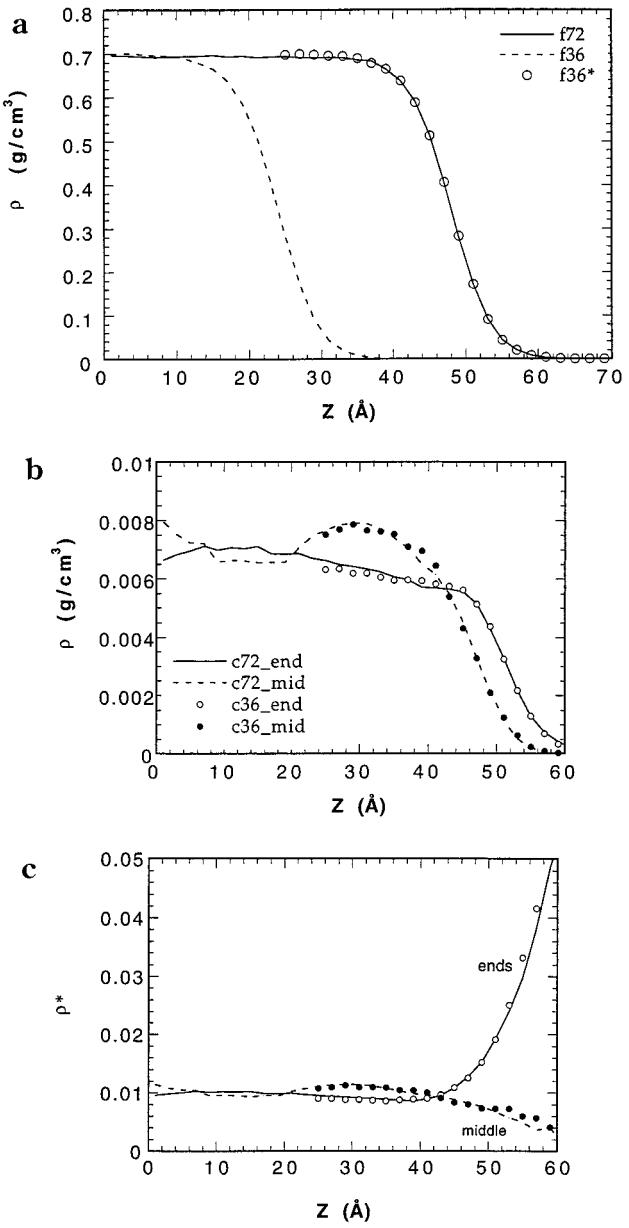

Figure 2. (a) Density profiles of two PE films at 509 K as a function of the distance from the center of mass in the Z direction (normal to the interfaces). The solid (f72) and dashed (f36) lines correspond to films which contain 72 and 36 chains of C_{99}, respectively. The circles are the data points of f36, shifted by 24 Å in the Z direction so that the interface of both films coincide. (b) The density profiles of the end (solid line) and middle (dashed line) beads of the f72 film. The open and full circles are the respective end and middle bead distributions for the f36 film, shifted in the Z direction. (c) ρ^* indicates that the distributions in part b are plotted after normalization by the density of beads in part a.

open circles represent the data points that form the profile of the thinner film f36, shifted in the Z direction by 24 Å so that the interfaces of the two films coincide. Thus, it is observed that f36 and f72 exhibit the same interfacial profile and differ only by the thickness of their bulk regions. This result, where the interfacial profiles from two independent simulations are almost identical, indicates that the errors are small on the scale of the properties being calculated. In the following paragraphs, we will analyze in more detail if any differences could be observed in the bulk and/or interfacial regions of these films.

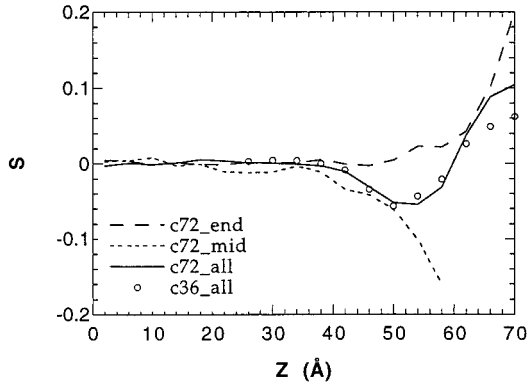

Figure 3. Orientation of the coarse-grained 2nnd bonds with the Z-axis (see text for definition). The solid line is obtained as an average over all bonds, whereas long and short dashed lines indicate the end and middle bonds of f72 film. The circles are the f36 film data points for all bonds (shifted in Z-direction).

Figure 2b gives the density profile of the end ($k = 1$ or 99) and middle carbon atoms ($k = 50$) across the films. The profiles of f72 are in agreement with those obtained in earlier simulations.[2,3] Both middle and end bead density approach bulk density divided by $N_C = 99$, i.e., the total number of carbon atoms in each chain. The small increase in middle bead density close to the center of the f72 film is indicative of some oscillatory behavior, which was also observed in MD simulations of short alkanes.[3] In Figure 2c, the bead density profiles are normalized by the total bead density in that bin, so that the distribution at the interface can be observed clearly. This is also typical in the sense that the end beads become more abundant closer to the vacuum. In terms of end and middle bead distributions, f36 exhibits characteristics quite similar to those of f72.

Orientation of Bonds. The order parameter defined as

$$S = {}^1/_2 \langle 3 (\cos^2\theta) - 1 \rangle \qquad (1)$$

is used for the determination of any orientational preferences of the bonds across the film. Here, θ is the angle between any bond and the Z axis (the normal to the interfaces). In Figure 3, the order parameter of bonds is plotted as a function of Z. The solid line represents the orientation of all the coarse-grained 2nnd bonds in f72, which correspond to bonds connecting i and $(i + 2)$ carbon atoms on the reverse-mapped chains. The long and short dashed lines are calculated for the 2nnd bonds at the ends and the middle of f72 chains, respectively. There is no preferred orientation in the bulk region of the film, since $S(Z) = 0$ for random orientation. Toward the interface, the middle bonds seem to prefer parallel orientation, whereas the end bonds tend to stick out to the vacuum by normal orientation to the surface. ($S = -{}^1/_2$ for perfect parallel and $S = 1$ for perpendicular orientations.) Therefore, these two opposite effects are averaged in the orientation of all bonds. All these results are in accordance with previous simulations.[2,3] In this calculation, larger bins of 4 Å thickness are used in order to get better statistics of middle bond orientation toward the interface. No difference is observed in the orientation of all bonds whether 2 or 4 Å bins are used. The open circles represent the data for all bonds of the f36 film, which seem to exhibit a behavior similar to that of f72.

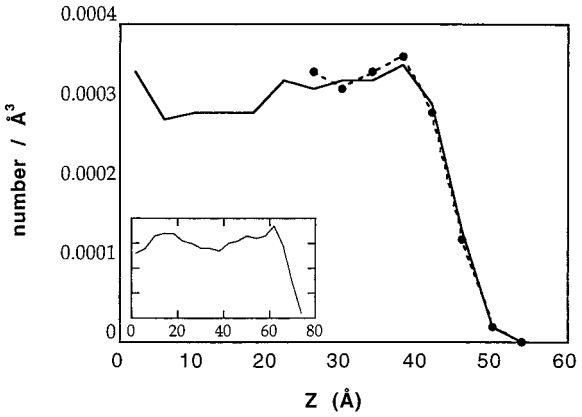

Figure 4. Center of mass distribution of the chains across the f72 (solid line) and f36 (dashed line with solid circles, data points shifted in *Z* direction) films. The number of chains in 4 Å bins is divided by the bin volume. The inset gives results from a film containing 108 chains under the same simulation conditions.

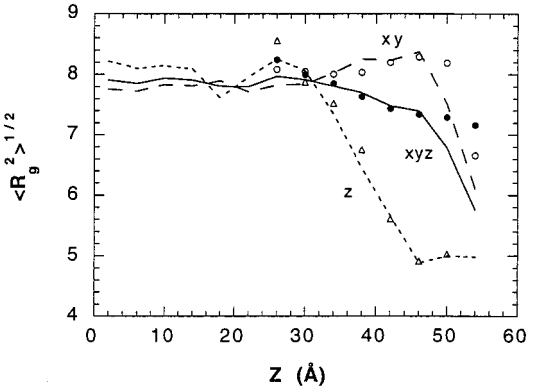

Figure 5. Components of the square-root of the mean-squared radius of gyration. Lines are drawn for f72 film, whereas points represent data from the f36 film, shifted in *Z*-direction for comparison. *xyz* refers to the square root of the one-third of the total-mean squared radius of gyration, whereas *xy* refers to the average of *X* and *Y* components and *z* refers to the *Z* component.

Chain Properties. In this section, we will look at the global equilibrium properties of the chains. In this section, 4 Å bins are used in the calculations to obtain reliable statistics. The center of mass profiles of the chains are plotted in Figure 4, expressed as the number of chains per volume of bin (Å^3). The profiles seem to be almost identical for f36 and f72. The increase in the density close to the center of f72 seems to accompany the similar increase in the middle bead distribution. Again, this result indicates that an oscillatory behavior might exist. Some preliminary simulations (run 1 in Table 2) with a film containing 108 chains at the same conditions, which is given in the inset of Figure 4, shows that this peak actually drops down. The oscillations exhibit a periodicity of $\sim 3\langle R_g^2 \rangle^{1/2}$. In previous MD simulations, less pronounced oscillations in the center of mass distributions of C_{20} have also been observed at 400 K.[3]

Figure 5 gives the components of the radius of gyration of the chains as a function of the *Z* coordinate of their center of mass. The solid line is the square root of the 1/3 rd of the total mean-squared radius of gyration for f72 chains. The long dashed line gives the square root of the average of *X* and *Y* components, whereas the short dashed lines gives the square root of the *Z* component of the total mean-squared radius of gyration for f72 chains. In the bulk region of f72, all three components seem to be close to a mean value of ~8 Å, which is in agreement with $(\langle R_g^2 \rangle/3)^{1/2}$ value calculated for the simulation. In the interface region, the *Z* component of the chains decreases, whereas, the X and Y components increase with no significant decrease in the total $\langle R_g^2 \rangle^{1/2}$. Very close to the vacuum side, all three components approach to ~6 Å, with a significant decrease in $(\langle R_g^2 \rangle/3)^{1/2}$. These results are in qualitative agreement with the MC simulations of Kumar et al.[2] using bead−spring model chains and the MD simulations on short-alkane films.[3]

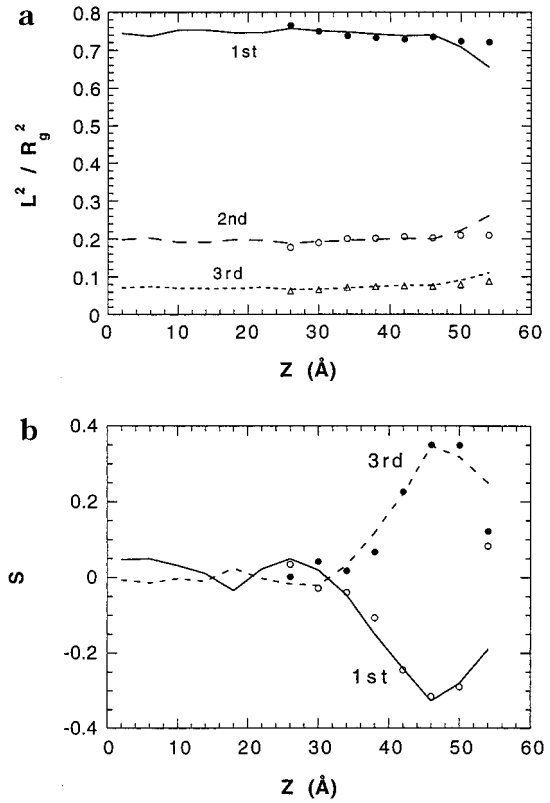

Figure 6. (a) The principal moments ($L_1^2 > L_2^2 > L_3^2$) of the chains (divided by the squared radius of gyration) as a function of *Z* for the center of mass of the chain. (b) The orientation of the first and third principal axis of the chains with the *Z* axis. In both figures, the lines are from the f72 film, whereas the points represent the data points of f36, shifted in the *Z* direction.

To define the shapes and orientation of the chains more clearly, the eigenvalues ($L_1^2 > L_2^2 > L_3^2$) of the radius of gyration tensor for each chain are calculated by converting to the principal axis system. Figure 6a shows the three eigenvalues (principal moments) of the chains normalized by their squared radius of gyration as a function of the *Z* coordinate of the center of mass for each chain. There is a slight change in the eigenvalues in the interface region of f72, most of which is occurring close to the vacuum side. The chain shapes can be better identified by the acylindricity and the asphericity values, which are defined as $c = (L_2^2 - L_3^2)$ and $b = L_1^2 - 1/2\,(L_2^2 + L_3^2)$, respectively. These values divided by the squared radius of gyration determine the extent of deviation from cylindrical and spherical shape in the range of 0 to 1. It is clear that the chains have a cylindrical shape with $\langle c/R_g^2 \rangle = 0.12$ in the bulk region, whereas the asphericity is quite high $\langle b/R_g^2 \rangle = 0.61$. Figure 6(b), on the other hand, displays the orientation

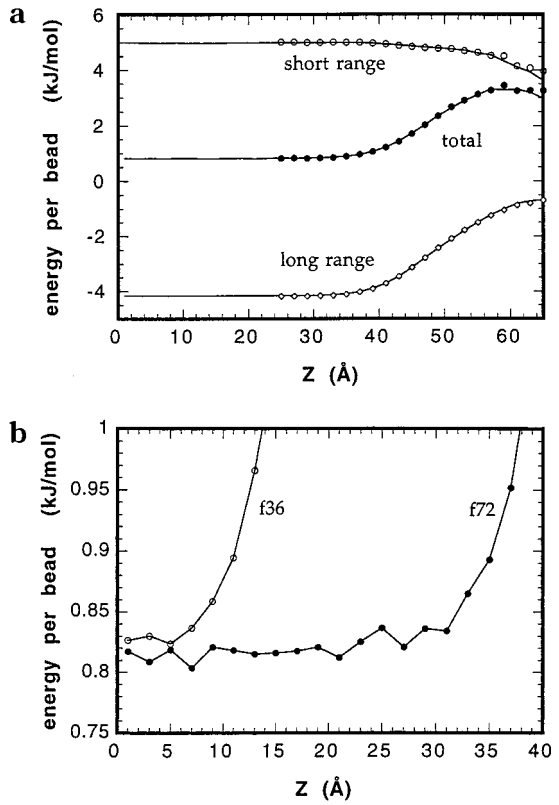

Figure 7. (a) Average short- and long-range and total energies per bead (in 2 Å bins) as a function of Z. The lines are from the f72 film, whereas the points represent the data points of f36, shifted in the Z direction. (b) The total energy per bead as a function of Z, starting from $Z = 0$. Only the bulk regions of f36 (empty circles) and f72 (solid circles) are blown up for details.

of the largest and the smallest eigen vectors of the chains, corresponding to L_1 and L_3, respectively, with the Z axis, defined as in eq 1. Both axes are randomly oriented in the bulk region, whereas there is a strong tendency for the first (largest) principal axis to orient parallel to the surface and the third (smallest) axis normal to the surface. This indicates that the chains reorient by aligning their longest axis along the cylindrical axis parallel to the interface. This reorientation of the chains, which is primarily responsible for the behavior observed in Figure 5, was observed in the studies on glassy atactic PP.[4] On the gas side of the interface this orientation behavior diminishes again.

In general, no significant differences between f36 and f72 films can be observed in terms of the global equilibrium properties, as well as the local properties.

Finally, our results on chain end and middle bead distributions, bond orientation and chain shapes are in conformity with the variable-density lattice model predictions of Theodorou,[18] even though the results of the latter model are presented for a short alkane (*n*-decane).

Surface Energies. The surface energy of the f72 film is calculated by comparing the total energy of the film to that of the bulk energy, which is extracted from the bulk region of the same film. Figure 7 a shows the short-range intramolecular (from the RIS model) and long-range (from the u_i) and total energies calculated in 2 Å bins as a function of Z direction. These energies are normalized by the number of beads in each bin. The short range energy per bead drops, while the long range energy per bead increases significantly in the interfacial region, the overall result being the increase in the total energy.

The potential energy part of the surface energy, γ, can be calculated by using the following relationship.

$$\gamma = \frac{\langle E_{2D}\rangle - \langle E_{3D}\rangle}{2A} \tag{2}$$

Here, $\langle E_{2D}\rangle$ and $\langle E_{3D}\rangle$ denote the average potential energies of the film and bulk, respectively. The surface area is denoted as $2A$, which is the sum of two interfaces. We can find $\langle E_{2D}\rangle$ directly from the thin film simulations. It is also possible to extract $\langle E_{3D}\rangle$ by using the energetics of the bulk region of the film. Specifically, the average energy per bead in the constant bulk region of Figure 7a is multiplied by the total number of beads in the system to obtain $\langle E_{3D}\rangle$. In Figure 7b, the bulk regions of f36 and f72 are magnified in order to view the constant portions of the total energy data from which $\langle E_{3D}\rangle$ can be extracted. f36 exhibits almost no constant region at all, whereas $Z < 22$ Å is used for calculating the bulk energy from f72. Using this formulation, a surface energy of 22.2 erg/cm^2 is calculated for f72. The experimental value[19] at this temperature is 23.4 erg/cm^2.

2. Two Films at Different Temperatures. In this section, we will compare the equilibrium properties of the films in runs 3 and 5, given in Table 2. Both films have the same periodic cross-sectional area (21 × 22 lattices) and number of chains. Run 3 is the same as the thinner film of 36 chains, described in the previous section. Run 5 is performed at a lower temperature of 400 K (slightly below the melting temperature of PE). There is a temperature difference of 109 °C between the two runs. Only the significant differences will be summarized below. Since the thermal expansion coefficient resulting from the set II long-range parameters is actually lower than that for PE (see Figure 1), the effects seen here may underestimate the real situation.

Density Profiles. Figure 8a gives a comparison of the density profiles of the films. As expected, the film at 400 K exhibits a higher bulk density (~0.72 g/cm^3) and a sharper interface. In Figure 8b, end and middle bead distributions across the films are plotted after normalization by the total bead densities. The end beads are more concentrated in the narrower interfacial region of the lower temperature film compared to the higher temperature.

Orientation of Bonds. In Figure 9, order parameters are plotted for all, end, and middle 2nnd bonds at 400 K. Here, the lines represent the film at 400 K, and for the film at 509 K only the data points for all bonds are included as empty circles. The ordering at the interface is much more effective at the lower temperature.

Chain Properties. The chain centers of mass distribution is given in Figure 10a at the two temperatures. Figure 10b exhibits the components of the mean squared radius of gyration for the film at 400 K. Comparison of the trend with that of Figure 5, in the previous section for $T = 509$, indicates that the orientation in the interfacial region at 400 K seems to be more pronounced. The shapes of the chains, i.e., the eigenvalues (not shown), stay almost constant at 400 K throughout the film except on the gas side of the interface, where there are not enough chains to obtain reliable statistics. The average acylindricity and asphericity values are $\langle c/$

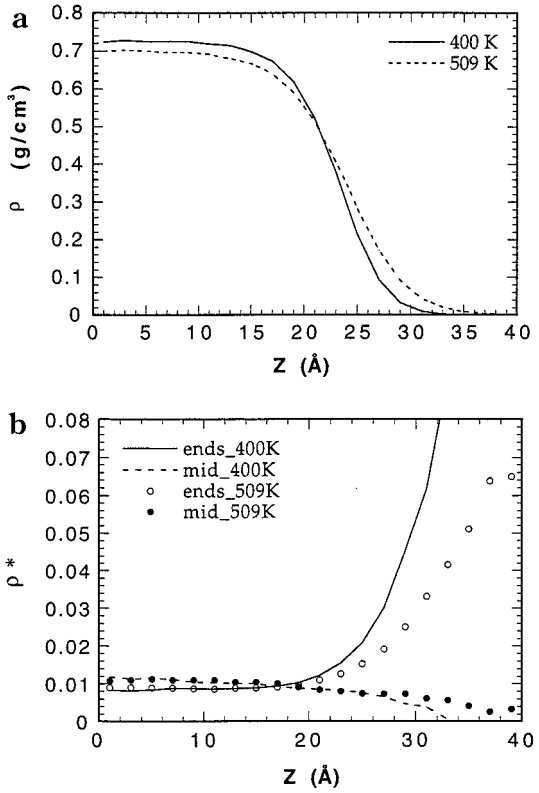

Figure 8. (a) Comparison of the density profiles of two 36-chain films at 400 K (solid line) and 509 K (dashed line). (b) End and middle bead density profiles as a function of Z at 400 (lines) and 509 K (circles). Data are normalized by the total bead density in each bin.

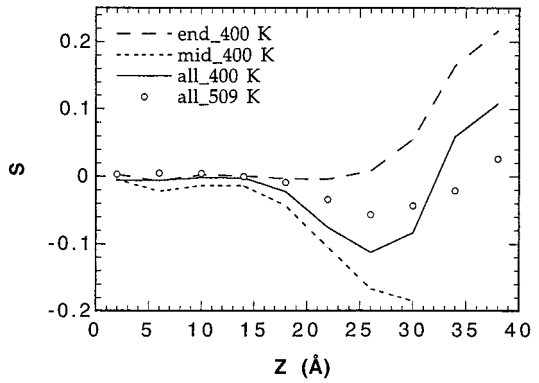

Figure 9. Orientation of the coarse-grained 2nnd bonds with the Z-axis (see text for definition). The solid line is obtained as an average over all bonds, whereas long and short dashed lines indicate the end and middle bonds for 36-chain film at 400 K. The circles are the 36-chain film data points for all bonds at 509 K.

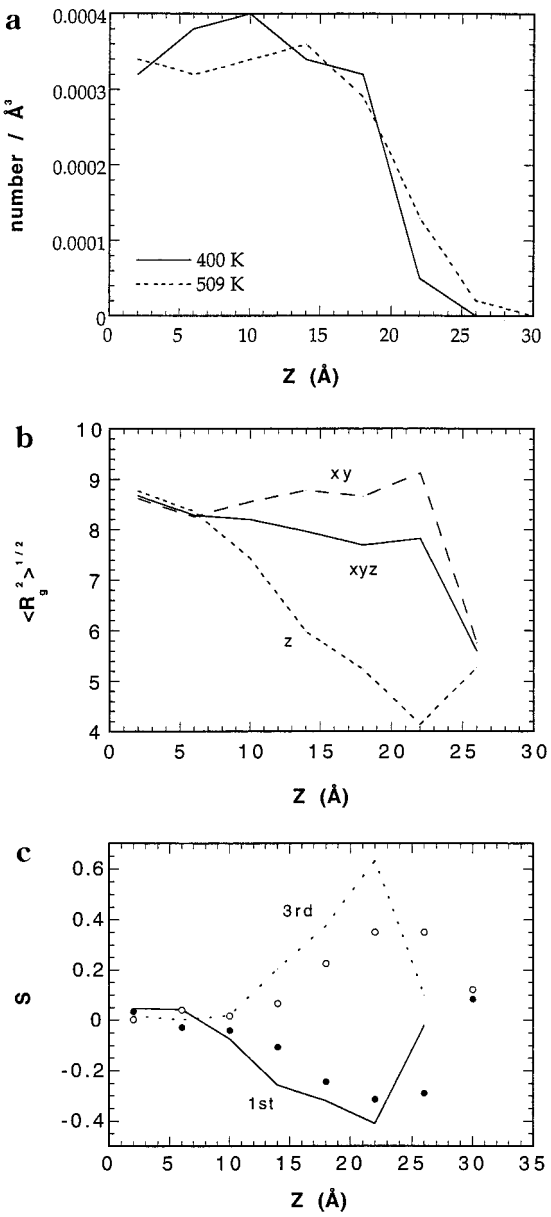

Figure 10. (a) Center of mass distribution of the chains across the 36-chain films at 400 K (solid line) and at 509 K (dashed line). The number of chains in 4 Å bins is divided by the bin volume. (b) Components of the square-root of the mean-squared radius of gyration for the 36-chain film at 400 K. (See Figure 5 for the definitions of *xyz*, *xy*, and *z* and for a comparison with the film at 509 K.) (c) The Orientation of the first and third principal axis of the chains with the Z axis. The lines are from the film at 400 K, whereas the points represent the data points of the film at 509 K.

$R_g^2\rangle = 0.12$ and $\langle b/R_g^2\rangle = 0.63$, respectively. The orientation of the first and third principal axes of the chains are compared at the different temperatures in Figure 10(c). The reorientation of the chains in the interface region is more significant at the lower temperature.

There is an additional remark to be made in this section about run 4, which is carried out at 443 K. Actually, two independent simulations are performed starting with different initial conformations. One of the initial conformations is an equilibrated snapshot from run 3 at 509 K, whereas the other is from run 5 at 400 K. Both of the snapshots are reequilibrated at 443 K, and the resulting structures exhibit almost identical properties in terms of density profiles and bond orientation profiles. The equilibrium distributions of the chains seem to be also converging for the two films, even though longer equilibration and analysis periods are necessary.

3. Analysis of Reverse-Mapped and Energy-Minimized Snapshots. In this section, some snapshots from run 8 in Table 2 are reverse mapped back to the tetrahedral lattice. Energy minimization (EM) of these snapshots is carried out by using Discover 3.0 with the CVFF force field after placing the hydrogen atoms onto the backbone carbon atoms. EM is performed till the gradient is less than 0.1 kcal/(mol Å) for each snapshot. The details for this procedure of obtaining

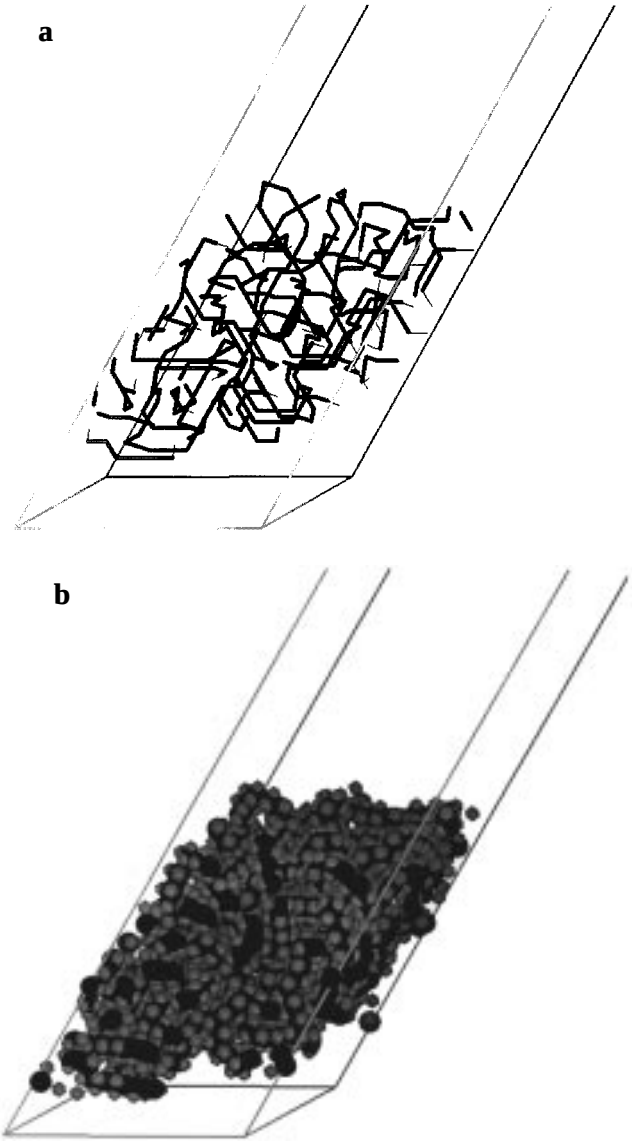

Figure 11. (a) Thin film snapshot on the 2nnd lattice from a nine-chain simulation at 443 K. (before reverse mapping) (b) Atomistic representation of the same snapshot after reverse mapping and energy minimization in continuous space. Carbon atoms (black) and hydrogens (gray) are indicated. (see text for details)

fully atomistic snapshots in continuous space can be found in ref 14. The previous application used a bulk system at constant density, but in the present simulation the density can change during EM. Therefore the temperature of the present film after EM is not as well defined as was the temperature (via the density) of the previous bulk system. The film in run 8 has a smaller cross-sectional area (925 Å^2 formed by 13 × 13 lattices) and thickness compared to those described in the previous sections. The smaller system size is chosen for carrying out efficient EM for the fully atomistic systems. However, EM for films containing more chains can be performed by using united atom force fields, in which the hydrogen atoms are collapsed on the backbone atoms.

Parts a and b of Figure 11 represent the same film snapshot on the 2nnd lattice before reverse mapping and in continuous space after EM, respectively. The dark solid lines in Figure 11a stand for the coarse grained 2nnd bonds. The black atoms in Figure 11b are the backbone carbons, whereas the gray atoms are the hydrogens.

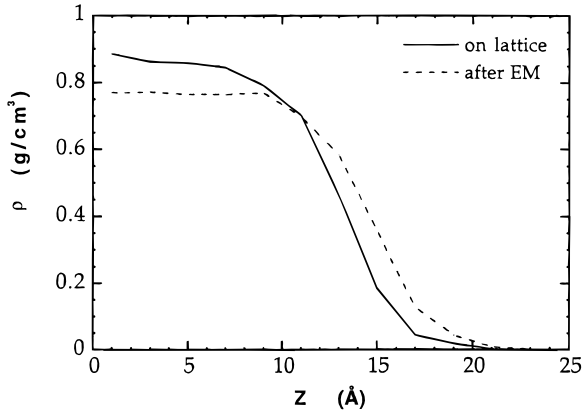

Figure 12. Comparison of the average density profiles of eight different snapshots on the 2nnd lattice and in continuous space (after EM). The films contain nine chains of C_{99} at 443 K.

Table 4. Average Energies of Bulk and Thin Film Snapshots (Nine Chains, Run 8)

	energy (kJ/mol)		
	film	bulk	difference
bond	364 ± 5	367 ± 6	−3
angle	1338 ± 39	1347 ± 66	−9
torsion	614 ± 34	689 ± 51	−75
nonbonded	−1272 ± 72	−1689 ± 37	417
tot.	1044 ± 115	713 ± 141	331

Figure 12 compares the average density profiles of 8 different film snapshots on the 2nnd lattice and after EM. It is observed that the film expands in the *Z* direction during EM. This is consistent with the fact that the bulk density of the film simulated by the parameter set I is higher than the experimental density of PE at 443 K (0.768 g/cm^3). Actually, the average density in the bulk region of the film snapshots decreases from 0.87 to 0.77 g/cm^3 during EM. In fact, 0.87 g/ cm^3 almost corresponds to the bulk density of amorphous PE at 293 K.

The potential energy part of the surface energy, γ, can be calculated directly from the average total energies (summation of the short and long-range energies on the 2nnd lattice) during the coarse-grained lattice simulations using eq 2. The important point is to choose a bulk simulation, which has the same density as the density of the thin film on the lattice (0.87 g/cm^3 at 443 K with set I, see Figure 11). The comparison of this run is, thus, made with a bulk simulation of nine chains at a density of 0.86 g/cm^3, carried out in a simulation box of 13 × 13 × 13 lattices. The surface energy is calculated as 32.2 erg/cm^2. The experimental surface energy for PE changes between 35.7 erg/cm^2 at 293 K and 27.2 erg/cm^2 at 443 K.[19]

An alternative method of calculating surface energies could be to use average energies of energy minimized snapshots in continuous space. In Table 4, a documentation of the components of internal energy, which are the bond stretching, bond bending, torsional, and van der Waals energies, is tabulated for thin film and bulk simulations. The tabulated energy values are the averages of nine different snapshots in each case. The bulk simulation in this table is a different run with a density of 0.75 g/cm^3 (nine chains of C_{99} in a box of 13 × 13 × 15 lattices), which is close to the average bulk density of the thin film after EM (0.77 g/cm^3). The

surface energy is calculated as 30.0 erg/cm^2 by this method. Since the surface energies from the simulation are close to the surface energies from experiment, the results imply that energy, not entropy, dominates the experimental surface energies. The nine snapshots chosen from the film and the bulk simulations are independent of each other, because the intervals between each snapshot are chosen such that the chain centers of mass on the average move at least about one radius of gyration in this period. The components of the potential energy indicate that the greatest contribution to the surface energy comes from the nonbonded interactions, which is partially offset by the decrease in torsional energies upon surface formation. The effect of the decrease in bond stretching and bond bending potentials seems negligible. These trends are qualitatively in agreement with the MD results of Misra *et al.*[6] on *cis*-PDB.

Concluding Remarks

It is possible to perform thin film simulations on the 2nnd lattice due to presence of cohesive long-range interactions in the model. The film chooses its own bulk density depending on the temperature and the long-range parameter set. In this respect, film simulations serve as a useful tool in fine-tuning the long-range interactions, i.e., choosing among the available parameter sets so that the specific polymer can be best described on the lattice. In this study, the parameter set II is found to be satisfactory for bulk simulations for PE, even though it underestimates the actual density and the thermal expansion coeffient.

Simulations with films of different thickness have not indicated any significant differences in the local and global characteristics of the chains. This comparison is carried out with films that contain 36 and 72 chains of C_{99} at 509 K. The major results can be summarized as follows:

The density profiles are hyperbolic. The end beads dominate at the interface.

The bonds tend to orient parallel to the surface in the interfacial region, whereas this behavior diminishes toward the gas side of the interface due to the end beads, which tend to stick out toward the vacuum and orient perpendicular to the surface.

There is an oscillatory behavior in the distribution of the chain centers of mass.

The chains tend to orient parallel to the surface with their largest principal axis lying along the surface, whereas no significant changes in the shapes of the chains can be seen throughout the film.

The surface energy calculated for the film containing 72 chains is close the experimental value.

Comparison of two films of 36 chains at 400 and 509 K indicates that the orientational preferences are more pronounced at the lower temperature on both local and global scales. The interface is sharper and the end beads are more abundant at the interface at 400 K.

All these results seem to be in line with previous MC and MD simulations.[1−3] The importance of this study is the fact that we are modeling PE films, which have quite large systems sizes. Although the simulations are carried out on a coarse-grained lattice, we can reverse-map any snapshot from the 2nnd lattice and minimize its energy in order to obtain equilibrated atomistic snapshots in continuous space. We have illustrated this aspect of our simulations using films that which contain thinner films with nine chains of C_{99}. The energetics of the reverse mapped snapshots are quite close to experimental surface energies.

In view of these results, it will be interesting to analyze the dynamics of these films, both on local and global scales. This issue of dynamics will be dealt in a subsequent paper.

References and Notes

(1) Madden, W. G. *J. Chem. Phys.* **1987,** *87*, 1405.
(2) Kumar, S. K.; Russell, T. P.; Hariharan, A. *Chem. Eng. Sci.* **1994**, *49*, 2899.
(3) Harris, J. G. *J. Phys. Chem.* **1992**, *96*, 5077.
(4) Mansfield, K. F.; Theodorou, D. N. *Macromolecules* **1990**, *23*, 4430.
(5) Mansfield, K. F.; Theodorou, D. N. *Macromolecules* **1991**, *24*, 6283.
(6) Misra, S.; Fleming III, P. D.; Mattice, W. L. *J. Comput.-Aided Mater. Des.* **1995**, *2*, 101.
(7) He, D., Reneker; D. H., Mattice, W. L. *Comput. Theor. Polym. Sci.* **1997**, *7*, 19.
(8) Rapold, R. F.; Mattice, W. L. *J. Chem. Soc., Faraday Trans.* **1995**, *91*, 2435.
(9) Rapold, R. F.; Mattice, W. L. *Macromolecules* **1996**, *29*, 2457.
(10) Doruker, P.; Rapold, R. F.; Mattice, W. L. *J. Chem. Phys.* **1996**, *104*, 8742.
(11) Flory, P. J. *Statistical Mechanics of Chain Molecules*; Wiley: New York, 1969.
(12) Mattice, W. L.; Suter, U. W. *Conformational Theory of Large Molecules. The Rotational Isomeric State Model in Macromolecular Systems*; Wiley, New York, 1994.
(13) Cho, J.; Mattice, W. L. *Macromolecules* **1997**, *30*, 637.
(14) Doruker, P.; Mattice, W. L. *Macromolecules* **1997**, *30*, 5520.
(15) Abe, A.; Jernigan, R. L.; Flory, P. J. *J. Am. Chem. Soc.* **1966**, *88*, 631.
(16) Hirschfelder, J. O.; Curtiss, C. F.; Bird, B. B. *Molecular Theory of Gases and Liquids*, Wiley; New York, 1954.
(17) Orwoll, R. A. In *Physical Properties of Polymers Handbook*; Mark, J. E., Ed.; American Institute of Physics: Woodbury, NY, 1996; p 81.
(18) Theodorou, D. N. *Macromolecules* **1989**, *22*, 4578.
(19) Wu, S. *J. Colloid Interface Sci.* **1969**, *31*, 153.

MA971322Z